PHYSICAL REVIEW B **82**, 075405 (2010)

Epitaxial growth of hexagonal boron nitride monolayers by a three-step boration-oxidation-nitration process

Frank Müller,[1,*,†] Stefan Hüfner,[1] Hermann Sachdev,[2,*,‡] Stefan Gsell,[3] and Matthias Schreck[3]
[1]*Experimental Physics, Faculty of Natural Sciences and Technology, Saarland University, 66123 Saarbrücken, Germany*
[2]*Inorganic Chemistry, Faculty of Natural Sciences and Technology, Saarland University, 66123 Saarbrücken, Germany*
[3]*Institute of Physics, University of Augsburg, 86135 Augsburg, Germany*
(Received 4 May 2010; revised manuscript received 24 June 2010; published 6 August 2010)

The formation of well-ordered monolayers of hexagonal boron nitride on the surface of a Rh/YSZ/Si(111) multilayer substrate via a three-step boration-oxidation-nitration process was investigated by x-ray photoelectron spectroscopy (XPS), x-ray photoelectron diffraction (XPD) and low-energy electron diffraction (LEED). The chemical vapor deposition (CVD) of trimethylborate $B(OCH_3)_3$ results in a selective decomposition of the precursor, leading to a dilute distribution of boron within the interstitials of the Rh lattice. After oxidation, the layer of a boron oxygen species of about 1 nm thickness can be transformed into a hexagonal monolayer of BN by annealing in NH_3 atmosphere. The results of the present study clearly show that the formation of BN monolayers is also possible when boron and nitrogen are provided successively from separate sources. This procedure represents an alternative routine for the preparation of well-ordered BN monolayers, which benefits from a strong reduction of hazardous potential and economic costs compared to the use of borazine as the current standard precursor.

DOI: 10.1103/PhysRevB.82.075405 PACS number(s): 61.46.−w, 62.23.Kn, 81.07.−b, 81.16.−c

I. INTRODUCTION

With increasing miniaturization in technology the engineering of future generations of electronic devices by applying standard techniques becomes more and more difficult, and especially after crossing the border to nanotechnology, the manufacturing of a particular design by "external" methods will reach its limits. Of course, a "message" can be written on the surface of a solid simply by aligning a few atoms with the tip in scanning tunneling microscopy (STM), but this way to manipulate surface structures is only appropriate for applications on a local scale rather than for the production of large-scale nanodevices.

Another way for the engineering of large scale nanostructures with a high degree of order is to use the phenomenon of self-assembly. This mechanism occurs during the epitaxial growth of thin films on substrates of different lattice parameters and/or different point symmetries. Depending on the lattice mismatch, periodicities in the range of a few Angstrøms (as for a usual crystal) can be extended to the range of a few nanometers, as given by the coincidence lattice of the film and the substrate. Additionally, the enlarged unit cells of such superstructures often exhibit complex topographies[1–4] that can be used as templates for the alignment of molecules,[5,6] a useful property, especially for the engineering of electronic devices in the post silicon era.

With respect to the latter aspect, the epitaxial growth of boron nitride (BN) on transition metal surfaces is of particular interest because it offers the possibility to get an insulator of exactly one monolayer that is isostructural to the new prodigy in material science and solid state physics, namely graphene.[7] The preparation of such BN monolayers benefits from the fact that the growth rate for BN strongly drops after the formation of the first layer, as shown by Nagashima *et al.*[8] for the growth of hexagonal BN monolayers on an isostructural Ni(111) surface (here, *hexagonal BN monolayer* refers to a graphenelike hexagonal sheet of *h*-BN or *r*-BN perpendicular to the *c* axis[9]). Especially after the discovery of a self-assembled superstructure of hexagonal BN monolayers on a Rh(111) surface by Corso *et al.*,[3] i.e., the so-called "*h-BN nanomesh,*" the growth of hexagonal BN monolayers gained new interest and investigations were extended to a large variety of transition metal surfaces under various aspects, such as lattice mismatch, substrate symmetry or bonding chemistry.[10–24]

All of these experimental investigations have in common that the preparation of the BN layers follows the same recipe: boron and nitrogen are provided via chemical vapor deposition (CVD) of similar precursors, namely benzene-like borazine $(HBNH)_3$ or trichloroborazine $(HBNCl)_3$, both containing a six membered B_3N_3 ring system as a structural motif also present in the resulting BN monolayer. From the preparative point of view, both precursors are easy to handle, at least on the laboratory scale: since the growth of BN monolayers is self-restricted[8] the preparation of a well-ordered hexagonal BN monolayer just requires opening an inlet valve for a short period. However, both precursors are not without problems, especially with respect to synthesis and hazardous properties.[25,26] Since these aspects are important for a large scale production of BN layers, we have looked for an alternative routine for the preparation of well-ordered BN monolayers, based on the use of widely used standard chemicals. In this study, we present a three-step boration-oxidation-nitration process that finally results in hexagonal BN monolayers of very high quality and that is based on the use of trimethylborate $B(OMe)_3$ (with $Me=CH_3$), oxygen O_2, ammonia NH_3 and a Rh/YSZ/Si(111) substrate as the low-cost and large-area counterpart of Rh(111) single crystals. The new synthesis route also provides a deeper insight into the self-organized formation of the hexagonal BN nanomesh pattern.

 ©2010 The American Physical Society

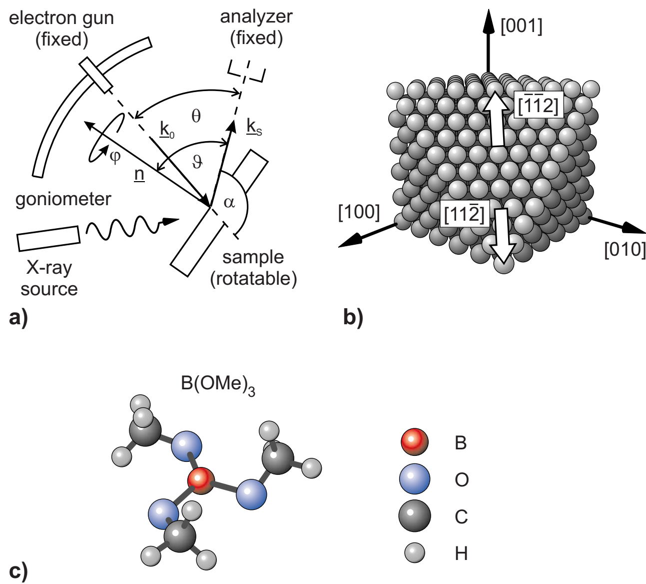

FIG. 1. (Color online) a) Experimental setup as described in the text, b) Structure of a (111) surface of a fcc crystal lattice. The $[\bar{1}\bar{1}2]$ and $[11\bar{2}]$ directions refer to the symmetry axes in $\underline{k}$-space with first-order LEED spots. c) Molecular structure of trimethylborate $B(OCH_3)_3$ used for the experiments.

II. EXPERIMENTAL

A. Experimental setup

The experiments were performed with a VG ESCA Mk II spectrometer which is equipped with a Osterwalder-type manipulator with two rotational degrees of freedom (polar angle ϑ, azimuthal angle φ). For angle-resolved experiments, such as x-ray photoelectron diffraction (XPD), angle-resolved ultraviolet photoelectron spectroscopy (ARUPS), Fermi surface mapping (FSM), and angle-resolved electron energy loss spectroscopy (AREELS), the whole 2π $\underline{k}$ space above the surface of the sample can be probed by a hemispherical 150°-type energy analyzer, as depicted in Fig. 1(a). For LEED, the intensity of the elastically scattered electrons at $\Delta E=0$ is recorded for the variation of the angular setting (ϑ,φ) by running the angular part and the spectroscopic part of the setup in the XPD and EELS mode, respectively, i.e., $I(\Delta E=0)$ is recorded for up to 30.000 angular settings (ϑ,φ).

A detailed description of the experimental setup, especially with respect to our method to record LEED patterns, can be found in Refs. 10, 12, and 27–29. Figure 1(b) shows the hexagonal (111) surface of the Rh lattice with the $[\bar{1}\bar{1}2]$ and $[11\bar{2}]$ directions in real space referring to the symmetry axis of the first order spots in reciprocal space. Figure 1(c) shows the molecular structure of the trimethylborate precursor, $B(OCH_3)_3$.

B. Rh/YSZ/Si(111) substrates

The Rh/YSZ/Si(111) substrates which we used instead of Rh(111) bulk single-crystals were already applied in previous studies to investigate the growth of hexagonal BN monolayers[10] by standard precursors as well as the growth of graphene monolayers.[30] The rhodium films prepared by e-beam evaporation from high-purity metal targets can compete with single crystals which frequently require long lasting annealing procedures to remove impurities, such as carbon, dissolved in the bulk crystals. The mosaic spread of the metal films in the range of few tenths of a degree is also comparable with typical bulk single crystals used for surface science studies. The preparation and properties of the Rh/YSZ/Si(111) substrates are described in Ref. 31 and differences to the surface of a Rh(111) single crystal, especially with respect to the growth of hexagonal BN, are discussed in detail in Ref. 10. Since the as-prepared substrates revealed only low O-1s and C-1s intensities in XPS, and due to the small thickness of the topmost Rh layer of 150 nm, the samples were cleaned by a soft Ar ion etching (~1 keV, 0.5 $\mu A/cm^2$ for a few minutes), followed by an annealing at about 900 K for 15 min. Residuals from carbon can be removed by additional annealing at 900 K within an oxygen atmosphere of about $4\cdot 10^{-7}$ mbar for 1 min (~20 L O_2), resulting in high quality Rh(111) surfaces.

C. Preparation of hexagonal BN layers

For the preparation of the hexagonal BN layers, the initial step consisted of the deposition of trimethylborate $B(OMe)_3$ (with $Me=CH_3$) which was previously cleaned by several cycles of liquid nitrogen freezing and subsequent evacuation of the glass tube down to $1\cdot 10^{-5}$ mbar. During the deposition, the glass tube as well as all gas lines in contact with the precursor were kept at about 330 K. $B(OMe)_3$ was let into the preparation chamber via a gas inlet, with the nozzle placed immediately above the surface of the substrate. During the deposition, the temperature of the Rh/YSZ/Si(111) multilayer substrate was set to 800 K and the pressure within the preparation chamber was $4.4\cdot 10^{-7}$ mbar for about 450 s, resulting in a nominal deposition of 150 L.

The second step of BN formation consisted of several oxidation cycles with the sample being annealed at 900 K in an oxygen atmosphere of about $4.4\cdot 10^{-7}$ mbar for about 75–150 s, resulting in nominal doses of 25–50 L O_2 for each cycle. The third step of BN formation consisted of several nitration cycles with the temperature also set to 900 K, but due to different reaction kinetics, the NH_3 pressure (the deposition time) had to be decreased (increased) by one order of magnitude to about $4.4\cdot 10^{-8}$ mbar (1500 s) to keep the same nominal dose of about 50 L NH_3 for each step of nitration.

III. RESULTS AND DISCUSSION

A. Formation of hexagonal BN monolayers by a three-step boration-oxidation-nitration process

1. Deposition of trimethylborate $B(OMe)_3$, *formation of boron rhodium compound*

The investigation of the CVD decay of the $B(OMe)_3$ precursor starts with a clean Rh surface with no detectable O-1s intensity and with only very small traces of C-1s from unavoidable residuals from adsorbates, as displayed by the XPS data in the bottom row in Fig. 2. The deposition of the

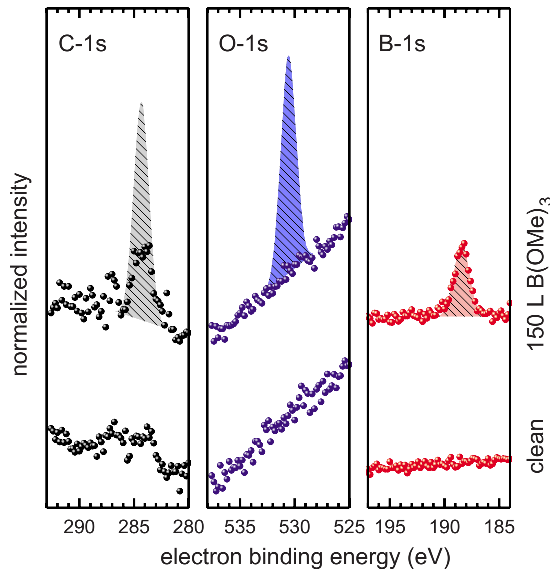

FIG. 2. (Color online) XPS data (Al-K$_\alpha$, $\hbar\omega=1486.6$ eV, normal emission) for C-1s, O1-s and B-1s for clean sample (bottom) and after deposition of 150 L $B(OCH_3)_3$ at 800 K (top) with normalized intensities displaying atomic ratios. The shaded areas represent the intensities that would be expected for the exact stoichiometry of the precursor. From the slight increase of C-1s intensity and the vanishing O-1s intensity, a complete decomposition of the precursor can be expected, see text.

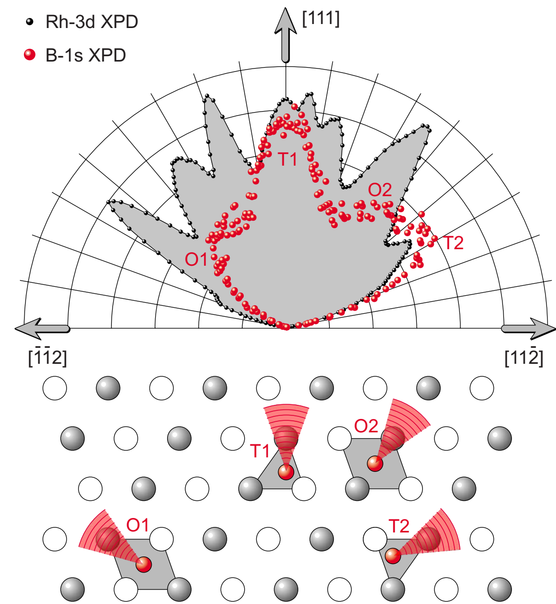

FIG. 3. (Color online) Angular intensity distributions (XPD) of Rh-3d photoelectrons (clean sample) and B-1s photoelectrons (after deposition of 150 L $B(OCH_3)_3$ at 800 K) in the $[\bar{1}\bar{1}2]-[111]-[11\bar{2}]$ plane, with surface normal along [111]. The Rh-3d intensity displays the forward scattering from the corresponding lattice plane, cf. cross section of lattice structure (the hollow circles represent Rh atoms from neighboring planes). The B-1s intensity mainly displays rather the forward scattering from the tetrahedral sites (T1, T2) than the scattering from the octahedral sites (O1, O2).

$B(OMe)_3$ precursor (150 L $B(OMe)_3$ at 800 K) then results in a distinct B-1s signal at 188.4 eV which is close to the value reported for boron segregation in a Rh foil.[32] Strikingly, neither an oxygen deposition nor a significant accumulation of carbon is detectable after the deposition (top row in Fig. 2). These findings give evidence that the decay of trimethylborate is based on the formation of a dilute "rhodium boride" phase and volatile species removing the oxygen and carbon present in the precursor.

Taking the B-1s intensity as a reference, the shaded areas in Fig. 2 represent the O-1s and C-1s intensities that are expected if the full C:O:B=3:3:1 stoichiometry of the precursor would be displayed in the XPS data after the CVD of $B(OMe)_3$. Surprisingly, the O-1s intensity still remains below the detection limit and only a small increase in the C-1s intensity is observed. Although the experimental C:B ratio is in the range of ~1:1, there is evidence that nearly a complete decomposition of the precursor takes place. For oxygen this is obvious from the lack of any signal. With respect to carbon, we refer to the following argument: According to the XPD data discussed below, the boron is embedded in the Rh lattice, and according to the increase of B-1s intensity during oxidation (cf. next section), only ~20% of the overall amount of boron is displayed by the XPS data in Fig. 2. Therefore, the experimental C:B=1:1 ratio rescales to C:B=0.2:1, i.e., even if the total amount of C-1s in Fig. 2 would result from the precursor, the total amount of carbon is only 6%–7% of that in the precursor (C:B=0.2:1 as rescaled experimental ratio vs. C:B=3:1 from stoichiometry of the precursor). If one refers just to the increase of the C-1s intensity in Fig. 2, the total amount of carbon that results from the precursor is further reduced to about 3%–4%. The observed decomposition of the precursor is an interesting result for material science, because it may offer an easy access to thin boride coatings for wear resistant materials.

Figure 3 shows the XPD data for Rh-3d and B-1s within the $[\bar{1}\bar{1}2]-[111]-[11\bar{2}]$ symmetry plane. For the clean Rh/YSZ/Si(111) crystal, the intensity distribution of the Rh-3d electrons exhibits all angular features that can be assigned to the main forward-scattering directions for this particular plane of an fcc lattice. After the deposition of the precursor, also the B-1s intensity shows an angular anisotropy, but compared to the distinct structures of the Rh-3d scattering, the B-1s intensity just provides a more diffuse scattering pattern with a distinct left-right asymmetry of the $[\bar{1}\bar{1}2]-[111]$ and $[111]-[11\bar{2}]$ sectors, respectively. Apart from a slight attenuation of the overall Rh-3d intensity, the Rh-3d scattering after the deposition (not shown) is nearly the same as for the clean sample. Therefore, a distribution of dilute boron within the Rh lattice has to be expected and B-B scattering can be neglected in a first approximation. According to the distinct asymmetry in the B-1s XPD pattern, it can be assumed that the boron atoms are rather located at the tetrahedral interstitials of the Rh lattice than at the octahedral sites. In Fig. 3, a section of the Rh $[\bar{1}\bar{1}2]-[111]-[11\bar{2}]$ plane is shown with dilute boron occupying both the tetrahedral as well as the octahedral sites. Regarding the next-neighbor B-Rh forward scattering, the tetrahedral sites would rather contribute to intensity maxima within the $[111]-[11\bar{2}]$ sector, while in the

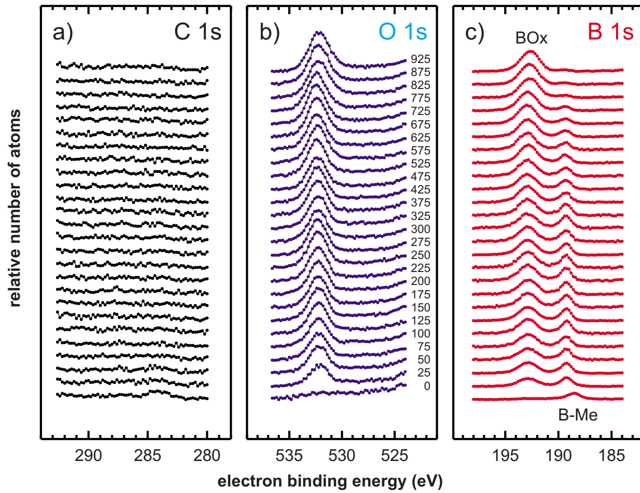

FIG. 4. (Color online) XPS data (Al-K_α, $\hbar\omega$=1486.6 eV) for a) C-1s, b) O1-s and c) B-1s during oxidation of the B-Rh surface with normalized intensities displaying atomic ratios. The oxygen dose in L is given by the numbers in b). After applying 25 L O_2, an additional B-1s intensity appears at 193 eV due to the formation of boron oxygen while the B-1s intensity from the initial B-Rh species slightly shifts to higher binding energies due to embedding of oxygen in the Rh lattice (dilute Rh-B-O). With increasing O_2 dose, the B-1s intensity is systematically shifted to the boron oxygen peak. Throughout the whole series, the C-1s intensity is at the detection limit.

$[\bar{1}\bar{1}2]-[111]$ sector only octahedral sites would contribute to the maxima. Since there is nearly no intensity modulation of B-1s intensity in the $[\bar{1}\bar{1}2]-[111]$ sector, the occupation of the octahedral sites is expected to be strongly suppressed.

2. Oxidation of the B-Rh surface, formation of a boron oxygen compound

According to the results of the previous section, the deposition of 150 L $B(OMe)_3$ at 800 K results in a dilute distribution of single boron atoms within the Rh lattice. In the following steps of preparation the sample is heated at 900 K in an oxygen atmosphere of about $4.4\cdot10^{-7}$ mbar in order to start a diffusion of the boron atoms that is directed toward the surface. Following this recipe, a boron oxygen compound is formed stepwise by applying doses of 25–50 L O_2 for each particular step of oxidation. Figure 4 shows the C-1s, O-1s and B-1s spectra (with the spectra at 0 L representing the data from the upper row of Fig. 2) that change considerably, even after applying the first dose of 25 L O_2. In Fig. 4(a), the C-1s intensity drops below the detection limit, which gives evidence that the further steps of preparation are not affected by any carbon impurities. The O-1s intensity in Fig. 4(b) shows a systematic increase and in the B-1s spectrum in Fig. 4(c) a second contribution appears at ~193 eV that can be assigned to the formation to a boron oxygen species.[33,34] Additionally, the presence of oxygen shifts the B-1s peak of the initial B-Rh species from 188.4 to 189.2 eV.

With increasing oxygen dose, no intensity is observed in the C-1s spectra in Fig. 4(a) while the O-1s intensity in Fig. 4(b) increases monotonically. In Fig. 4(c), the B-1s contribution at higher binding energy (boron oxygen species) also increases monotonically while the B-1s contribution at lower binding energy (B-Rh species) initially remains constant before it starts to drop and finally vanishes. Comparing the B-1s intensities of the initial surface (only B-Rh species) and after full oxidation at about 925 L O_2 (only boron oxygen species) there is an overall increase of boron intensity to about 500% during oxidation, although no additional boron was provided. Therefore, the overall amount of boron, as deposited by applying 150 L $B(OMe)_3$ in Sec. III A 1, is distributed deep within the Rh lattice and due to the high surface sensitivity of the technique, only a small fraction of boron is seen in Fig. 2 after the deposition of the precursor. Concerning the absence of any C-1s intensity even after the first dose of oxygen, two different scenarios may be discussed: In the first one, carbon is only present at the surface

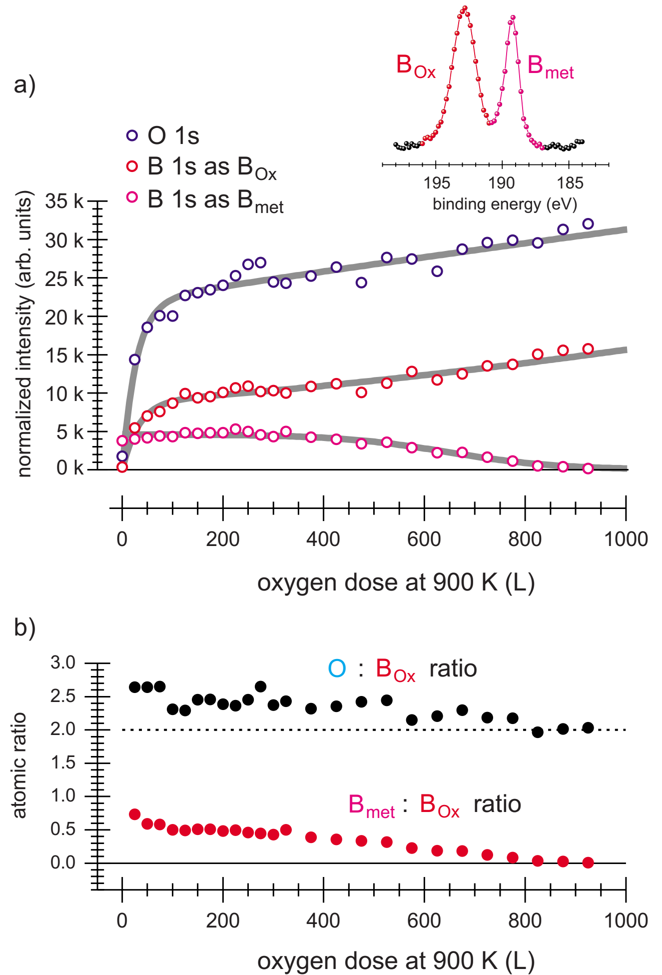

FIG. 5. (Color online) Quantitative analysis of the O-1s and B-1s intensities from Fig. 4. With increasing oxygen dose, the intensities from O-1s and the boron oxygen related part (B_{Ox}) of B-1s in a) are running parallel, while the B-Rh related part (B_{met}) of the B-1s intensity starts with constant values and finally drops to zero (gray lines are just a guide to the eye). In b), the ratio of O-1s intensity and boron oxygen related B-1s intensity approaches a 2:1 distribution, indicating the formation of a BO_2 species, such as metaboronacid. With increasing oxygen dose, the whole B-1s intensity from B_{met} is transformed to B-1s intensity from B_{Ox}.

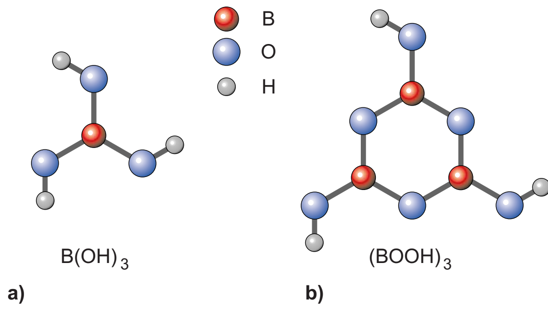

FIG. 6. (Color online) Molecular structures of a) orthoboronacid and b) metaboronacid with similar oxygen configuration of the boron atom, but different B:O ratios, 1:3 in a) and 1:2 in b), respectively. According to the results from Fig. 5, the formation of a glasslike layer by metaboronacid is expected.

and not dissolved in the bulk of the Rh film. As a consequence, the C-1s intensity in Fig. 2 displays the full amount of carbon present on the substrate in contrast to the B-1s intensity in Fig. 2, which represents only 20% of the overall amount of boron. As discussed in the previous section this results in a C:B ratio of 0.2:1. In an alternative scenario, carbon is distributed in the bulk of the metal film similar to boron. However, in contrast to boron which forms a stable oxide after diffusion to the surface, carbon forms volatile species, such as CO, which immediately desorb from the surface at the high process temperature. During all the further preparation steps the carbon signal was below the detection limit of XPS. This indicates that the type of the initial carbon distribution does not play any significant role in the formation of the BN nanomesh during the oxidation process.[35]

For a quantitative analysis, the intensities from Fig. 4 are compared in Fig. 5. In Fig. 5(a), the B-1s intensity from the oxygen species runs nearly parallel to the O-1s intensity, and the ratio of both curves in Fig. 5(b) predicts the formation of a boron oxygen species with B:O=1:2 ratio after full oxidation. The B-1s intensity from the Rh-B species in Fig. 5(a) starts with a constant value and finally drops to zero, indicating that the portion of boron that is transformed from the Rh-B species into boron oxygen is first replaced by a diffusion of boron from the bulk to the surface. When this source of boron starts to get exhausted, the further formation of the boron oxygen species finally causes the Rh-B species to vanish.

For the boron oxygen species in Fig. 4(c), the observed binding energy of about 193 eV is characteristic for, e.g., orthoboric acid, $B(OH)_3$,[34,36] with a B:O=1:3 ratio, as depicted in Fig. 6(a). This ratio deviates from the experimental B:O=1:2 ratio in Fig. 5(b), and therefore, we assume the formation of meta boric acid, $(BOOH)_3$, which provides the observed B:O=1:2 ratio,[36] as depicted in Fig. 6(b). Since the chemical coordination of boron is similar for both compounds (threefold sp^2-type coordination of boron by oxygen) the observed binding energy is expected to be also characteristic for meta boric acid. At this stage, there is no clear evidence where the hydrogen that is needed to form the boric acid finally comes from. However, in Ref. 35 it is proposed that boron hydride species (such as, e.g., BH_3) can form as

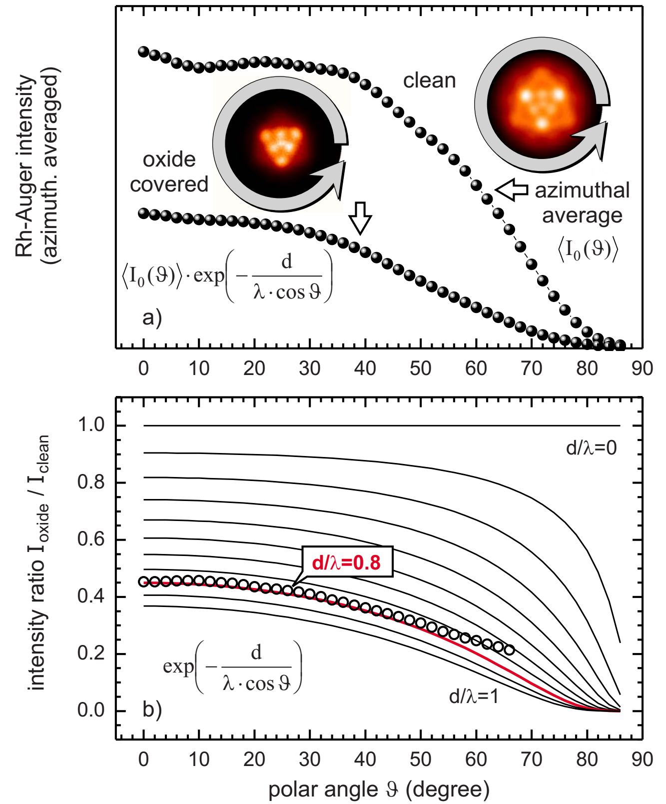

FIG. 7. (Color online) Approximation of the thickness of the boron oxygen layer by the attenuation of photoelectron intensity of the Rh surface. In a), forward scattering from the crystalline Rh surface is reduced by using electrons with small kinetic energies (here Rh-MVV Auger electrons, $E_{kin} \sim 300$ eV) at full angular apertures and by azimuthal averaging of the 2π diffraction patterns (gray dots). In b), the ratio of the azimuthally averaged polar distributions is compared to the factor $\exp(-d/\lambda \cos \vartheta)$ for d/λ ranging from 0 to 1 (in steps of 0.1) with d describing the thickness of the boron oxygen layer and λ describing the mean free path of the electrons (~1 nm). The thickness of the boron oxygen layer can be approximated as d ~8 Å ~1 nm.

intermediates during the decay of the trimethylborate precursor. If a dehydrogenation of these species (or even of the initial methyl groups of the precursor) takes place on the metal surface, hydrogen may be trapped in the interstitials of the substrate similar to boron. Of course, hydride formation usually requires enhanced pressure because otherwise hydrogen will be released,[37] but the partial occupation of the Rh interstitials by boron may inhibit an interstitial hopping of hydrogen. During oxidation, both elements are then released simultaneously to form the meta boric acid. Since hydrogen cannot be displayed by XPS, this question cannot be answered unambiguously and may be the object of a separate study.

For an estimation of the thickness of the boron oxygen layer, the attenuation of the photoelectron intensity from Rh is compared for the clean and the boron oxygen covered surface. In order to reduce angular intensity modulations by forward scattering, the intensity of the Rh MVV-Auger electrons with low kinetic energies (~300 eV for Al-K_α radiation) was recorded for full angular apertures. Since the XPD

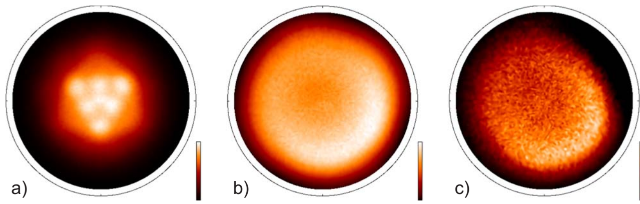

FIG. 8. (Color online) X-ray photoelectron diffraction (XPD) patterns (Al-K_α, stereographic projection) of a) Rh-MVV Auger, b) O-1s and c) B-1s for a ∼1 nm boron oxygen layer on Rh/YSZ/Si(111). In contrast to the Rh intensity in a), the O-1s and B-1s intensities in b)-c) display no distinct intensity modulation due to forward scattering, indicating the absence of crystalline order in the glasslike boron oxygen film. In b) and c), the azimuthal intensity modulations just result from the shape of the sample without azimuthal symmetry. Compared to the crystalline intensity modulation in a), the amplitude of these extrinsic modulations is lower by more than one order of magnitude.

patterns in Fig. 7 still display distinct intensity modulations by forward scattering, the data were azimuthally averaged. For a boron oxygen layer of thickness d, the polar intensity distribution of the clean surface $\langle I_0(\vartheta)\rangle$ is then attenuated by

$$\langle I(\vartheta)\rangle = \langle I_0(\vartheta)\rangle \cdot \exp\left(-\frac{d}{\lambda \cdot \cos\vartheta}\right)$$

for a particular polar angle ϑ, with λ describing the mean free path of the electrons ($\lambda \sim 1$ nm according to the so-called "universal curve"[38]). The ratio of the polar intensity distribution for the clean and boron oxygen covered surface in Fig. 7 results in a mean film thickness of

$$d_{\text{oxide}} = 0.8 \cdot \lambda \sim 8 \text{ Å}.$$

In contrast to the crystalline order of the Rh surface, as displayed by the XPD pattern of the Rh-MVV-Auger electrons in Fig. 8(a), no ordering can be observed for the boron oxygen film. The corresponding XPD patterns for O-1s and B-1s in Figs. 8(b) and 8(c) do not exhibit any intensity modulations, indicating the formation of a glasslike boron oxygen layer, as, e.g., by meta boric acid.

3. Nitration of the boron oxygen layer, formation of hexagonal BN monolayers

In the last preparation step the boron oxygen film can be transformed to a hexagonal BN monolayer by successive nitration in NH_3 atmosphere at 900 K. Compared to the oxidation of the previous section, nitration seems to be driven by much slower reaction kinetics. The best results were obtained by increasing/decreasing the reaction time/pressure by at least one order of magnitude compared to the settings in the oxidation process in order to have the same dosage for each step of preparation (oxidation at $4.4 \cdot 10^{-7}$ mbar O_2 for 150 s for 50 L vs. $4.4 \cdot 10^{-8}$ mbar NH_3 for 1500 s for 50 L). Following this procedure, it is possible to transform the disordered boron oxygen layer completely into a well-ordered hexagonal BN monolayer.

Figure 9 shows the C-1s, O-1s, N-1s, and B-1s spectra by applying NH_3 in doses of 50 L, with the spectra at 0 L NH_3

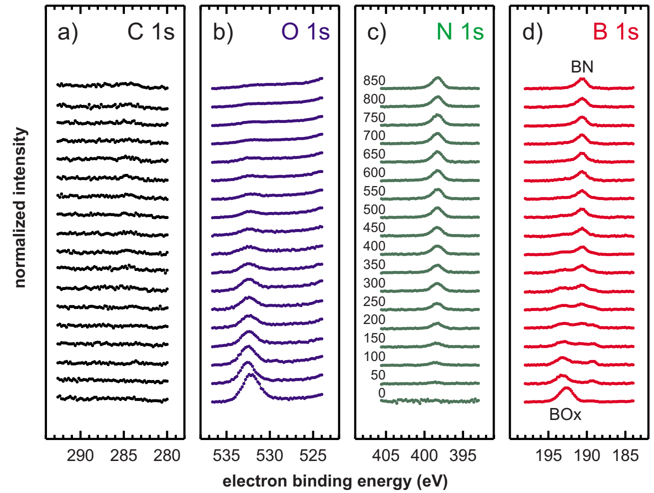

FIG. 9. (Color online) XPS data (Al-K_α, $\hbar\omega = 1486.6$ eV) for a) C-1s, b) O1-s, c) N-1s and d) B-1s during nitration of the boron oxygen surface with normalized intensities displaying atomic ratios. The NH_3 dose in L is given by the numbers in c). With increasing NH_3 dose, the O-1s intensity in b) decreases as the N-1s intensity in c) increases, while the B-1s peak due to the boron oxygen species at ∼193 eV is completely transferred to 190.6 eV as characteristic for the formation of BN. Throughout the whole series, the C-1s intensity in a) is at the detection limit.

representing the spectra for full oxidation at 925 L O_2 from Fig. 4. Similar to oxidation, the C-1s intensity in Fig. 9(a) is at the detection limit throughout the whole series. With increasing NH_3 dose, the initial O-1s intensity in Fig. 9(b) finally drops to zero, while in Fig. 9(c), an N-1s peak increases to saturation at the BN-like energy of 398.2 eV.[11] The behavior of the B-1s intensity in Fig. 9(d) is similar to that in the oxidation series, i.e., a second peaks appears, but now, the intensity is shifted from higher binding energy to lower binding energy at ∼ 190.6 eV due to the formation of BN.[11,39] In contrast to oxidation, the overall B-1s intensity slightly decreases, probably by the formation of volatile boron species during the boron oxygen—BN transformation, as discussed in Ref. 9.

In addition to the observed BN-like binding energies for N-1s and B-1s, as observed in Figs. 9(c) and 9(d), the formation of BN is also confirmed by the quantitative analysis of the N-1s and B-1s intensities. In Fig. 10, the normalized B-1s and N-1s intensities converge to a common value and as soon as the O-1s intensity disappears, the B:N ratio is close to unity.

Estimating the thickness of the BN coverage in the same way as the thickness of the boron oxygen layer in the previous section, the attenuation of the Rh intensity in Fig. 11 results in a thickness of about

$$d_{\text{BN}} = 0.2 \cdot \lambda - 0.3 \cdot \lambda \sim 2-3 \text{ Å}.$$

Taking the interlayer spacing of bulk *h*-BN along the *c* axis as a reference (∼3 Å), this thickness corresponds to a nominal coverage by about 2/3–1 monolayers of BN. Taking the uncertainty of the exact value for λ into account,[38] this result is in accordance with a monolayer coverage of BN.

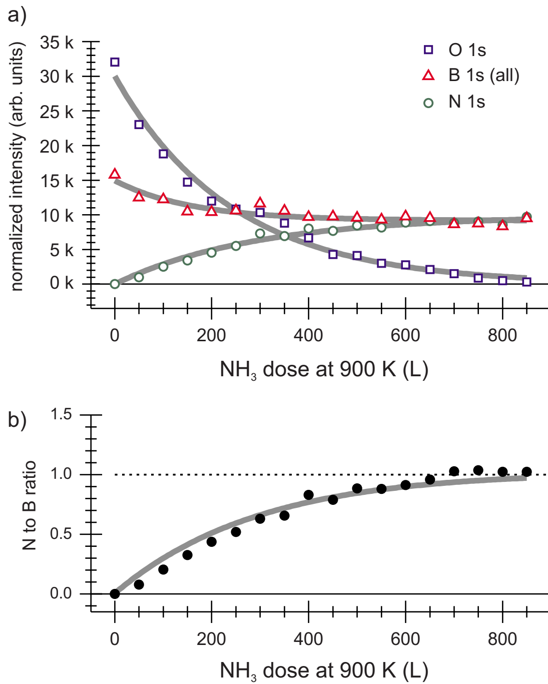

FIG. 10. (Color online) a) Quantitative analysis of the O-1s (blue square), B-1s (red triangle) and N-1s (green circle) intensities from Fig. 9. With increasing NH_3 dose, the O-1s intensity monotonically drops to zero, while the B-1s and N-1s intensities approach a common value (gray lines are just a guide to the eye). b) The formation of boron nitride BN is indicated by the B:N=1:1 ratio.

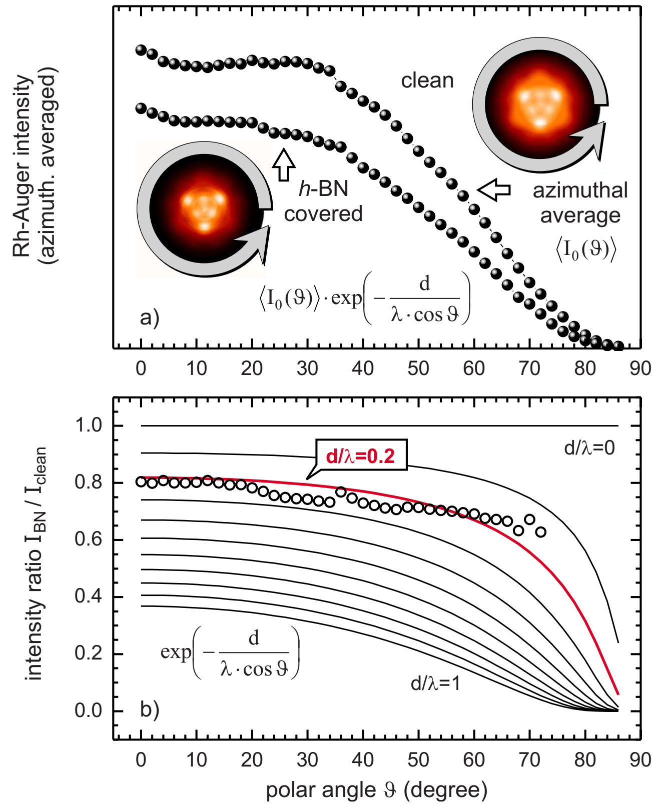

FIG. 11. (Color online) Approximation of the thickness of the boron nitride layer by the attenuation of photoelectron intensity of the Rh surface. a), same as in Fig. 7(a) for clean and BN-covered substrate. b), same as in Fig. 7(b). Here, the experimental intensity ratio results in a thickness of about d ~2-3 Å for the BN layer.

4. Surface structures

For a qualitative interpretation of the surface structures Fig. 12 compares the LEED patterns in the range of the first order spots. For the clean Rh surface, Fig. 12(a) provides a sharp LEED pattern with a sixfold arrangement of distinct spots with threefold intensity distribution, indicating that the clean substrate exhibits a well-ordered Rh(111) surface. After the deposition of the $B(OMe)_3$ precursor, the LEED pattern is nearly the same (not shown), except a slightly reduced peak-to-background ratio due to the dilute distribution of boron within the intersticials of the Rh lattice, as discussed in Sec. III A 1. After oxidation, the LEED pattern in Fig. 12(b) displays a diffuse intensity distribution due to the formation of a disordered boron oxygen layer of 8 Å thickness, as discussed in Sec. III A 2. After nitration of the boron oxygen layer, the formation of 2/3–1 monolayer of BN (cf. Sec. III A 3) then results in an increased peak-to-background ratio in Fig. 12(c), indicating that the disordered boron oxygen film is transformed into a well-ordered hexagonal BN monolayer. Compared to the clean Rh/YSZ/Si(111) surface in Fig. 12(a), the principal spots from the Rh lattice are now surrounded by a sixfold arrangement of additional intensity, as indicated in Fig. 12(d). These spots result from the BN/Rh(111) coincidence lattice and display the formation of the BN nanomesh (see Ref. 10 and references therein).

For a quantitative analysis, the polar intensity distributions along the $[\bar{1}\bar{1}2]$ axis [as indicated by the gray area in Fig. 12(a)], are compared in Fig. 13. The high degree of order for the clean Rh surface and the BN nanomesh on Rh/YSZ/Si(111) is displayed by the nearly vanishing background intensity in Fig. 13(a). In contrast, the disordered boron oxygen layer from Sec. III A 2 strongly suppresses the substrate spots, and the LEED profile is dominated by a high background. Since the lattice mismatch of the hexagonal BN and the Rh(111) lattice determines the size of the superstructure via the $(n+1\times n+1)/(n\times n)$ coincidence lattice, the spacing of the non-integral superstructure spots are distributed in fraction of 1/n in $\underline{k}$ space if the (00) and (10) spots of the substrate are set to $\Delta q^{\parallel}=0$ and $\Delta q^{\parallel}=1$, respectively. Figure 13(b) and 13(c) show the LEED profiles of the (00) spot and the (10) spot along the $[\bar{1}\bar{1}2]$ direction with the red lines representing the peak positions for $n=12$ and the blue lines representing the peak positions for $n=13$. Figure 13(b) and 13(c) give evidence that the superstructure spots are distributed rather in fractions of 1/13 than in fractions of 1/12, i.e., for the Rh/YSZ/Si(111) multilayer substrate, the size of the BN nanomesh is increased by one unit cell compared to a Rh(111) single crystal surface.[3] This phenomenon, as recently also observed for the growth of hexagonal BN layers on Rh/YSZ/Si(111) by using a borazine precursor, can be attributed to the different thermal properties of the Rh/YSZ/Si(111) multilayer system.[10] However, it has to be stated, that the observation of a $(14\times 14)/(13\times 13)$ superstructure is not a unique result. Throughout the preparation of a large variety

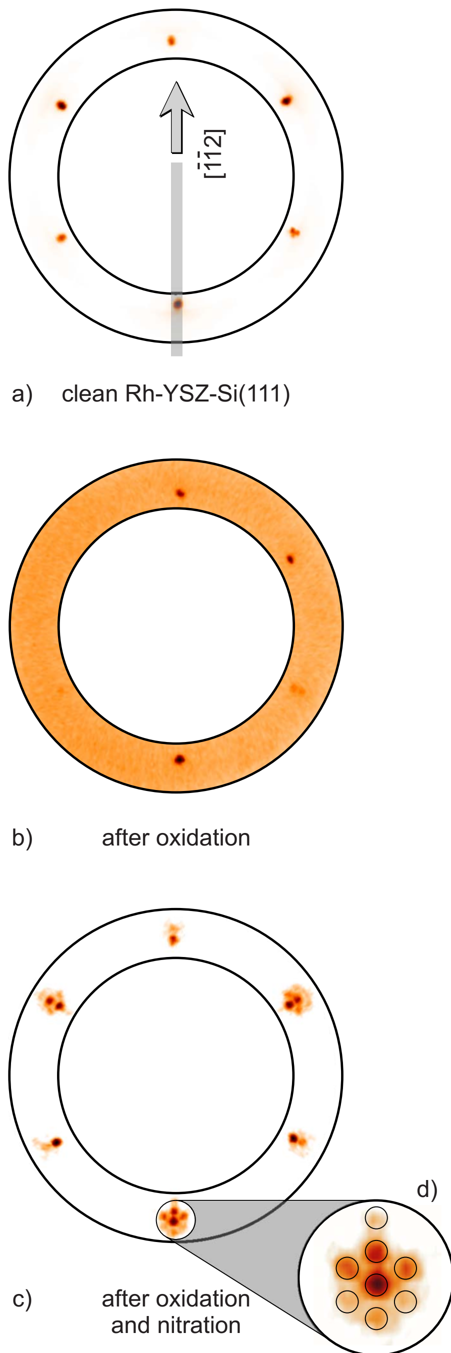

FIG. 12. (Color online) LEED patterns of a) clean Rh/YSZ/Si(111) surface, b) after formation of ~1 nm glasslike boron oxygen layer and c) after formation of ~1 monolayer BN after nitration of b). The formation of the hexagonal BN/Rh(111) Moiré pattern is seen by the additional sixfold intensity distribution of nonintegral spots around the principal spots, see also d).

of BN/Rh/YSZ/Si(111) layers, the size of the superstructure can vary between $(14\times14)/(13\times13)$ or a mixture of $(14\times14)/(13\times13)$ and $(13\times13)/(12\times12)$, i.e., the distribution of the superstructure spots is non-equidistant in the latter case, even if the parameters of preparation are fixed within the experimental error bars. However, apart from the size of the superstructure, the LEED data from Figs. 12 and 13 give clear evidence that the three-step boration-oxidation-nitration

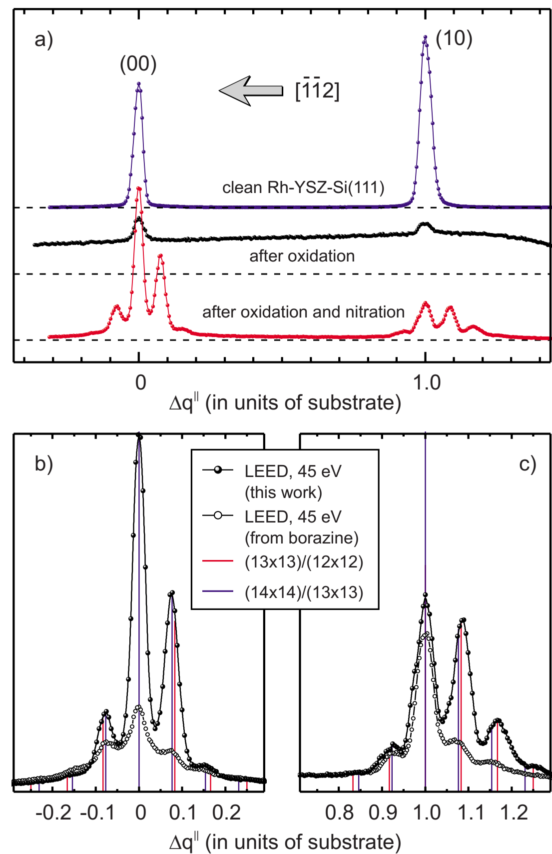

FIG. 13. (Color online) Quantitative analysis of the LEED profiles along the $[\bar{1}\bar{1}2]$ direction. In a), the high degree of order for the clean Rh/YSZ/Si(111) surface (top) and the BN/Rh/YSZ/Si(111) surface is displayed by the nearly vanishing background intensities. In contrast, after oxidation, the disordered glass-like boron oxygen layer causes the LEED profile (middle) to be dominated by background intensity. b) Spot profiles of the (00) spot along $[\bar{1}\bar{1}2]$ with non-integral intensities by the BN/Rh superstructure. c) Same as b) for (10) spot. In b-c, the spot profiles are compared to those obtained in Ref. 10 from a BN monolayer that was prepared by CVD of borazine.

process offers a viable route for the formation of well-ordered hexagonal BN monolayers. For comparison, Fig. 13(b) and 13(c) show the LEED profiles that are obtained by the same set-up when the BN/Rh/YSZ/Si(111) layer is prepared by CVD of borazine.[10] The formation of BN on Rh/YSZ/Si(111) by the three-step process is summarized in Fig. 14. Of course, this mechanism is expected to work also for a Rh(111) single crystal surface

B. Formation of hexagonal BN layers by a two-step boration-nitration process

In a second attempt, it was tried to grow hexagonal BN monolayers by an analog two-step boration-nitration process without an intermediate oxidation of the initial B-Rh compound. The deposition/decomposition of the $B(OMe)_3$ precursor and the nitration of the resulting B-Rh surfaces were similar to the procedures described in Sec. III A 1 and III A 3, respectively. Figure 15 shows the spectral series of

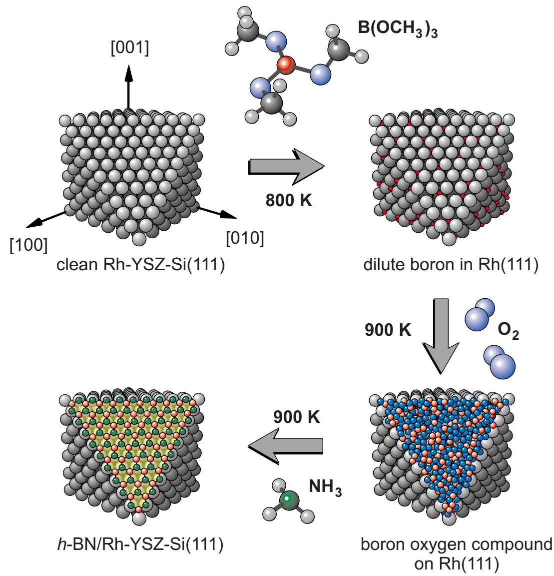

FIG. 14. (Color online) Schematic drawing of the three-step process for the formation of hexagonal BN monolayers.

the C-1s, O-1s, N-1s and B-1s peaks for successive nitration of the B-Rh compound by NH_3 at 900 K. Similar to the three-step boration-oxidation-nitration process, the B-1s spectra in Fig. 15(d) exhibit an additional contribution that can be assigned to the formation of a hexagonal BN layer, but in contrast to the three-step process, it is not possible to transform the B-1s intensity from the B-Rh species completely into B-1s intensity from BN. With increasing NH_3 dosage, both B-1s peaks finally display a constant intensity ratio. By comparing the BN related B-1s intensity at about

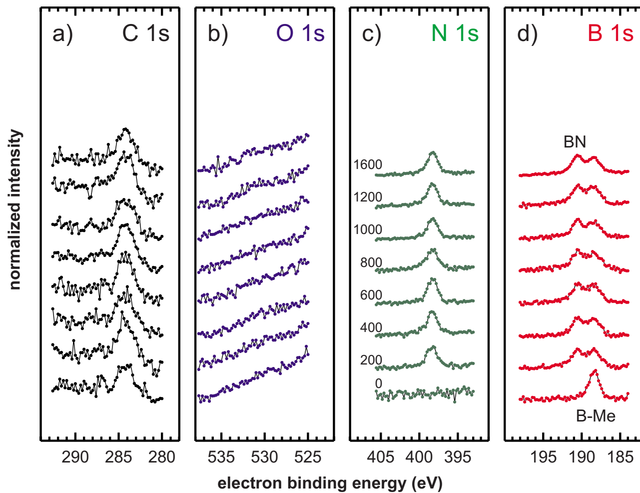

FIG. 15. (Color online) XPS data (Al-K$_\alpha$, $\hbar\omega$=1486.6 eV) for a) C-1s, b) O1-s, c) N-1s and d) B-1s after deposition of $B(OCH_3)_3$ and during nitration within the two-step process without intermediate oxidation with normalized intensities displaying atomic ratios. The numbers in c) indicate the NH_3 dose in L. Although BN is formed, it is not possible to extract all of the B-Rh related boron species out of the Rh lattice in d). In contrast to the three-step process, the surfaces exhibits large amounts of carbon impurities in a).

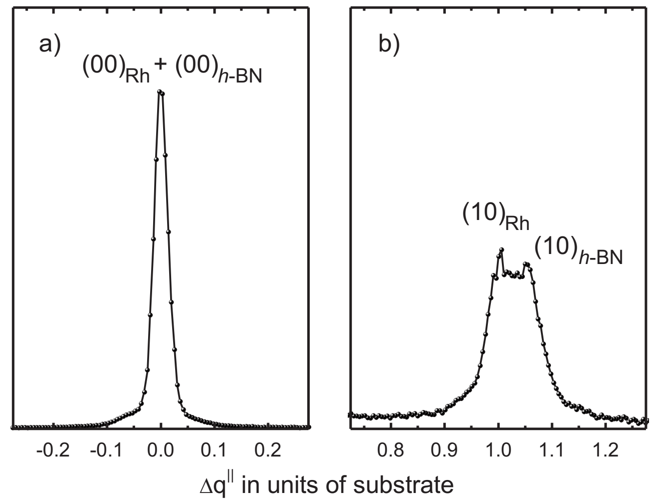

FIG. 16. LEED profiles along $[\bar{1}\bar{1}2]$ of a) (00) spot and b) (10) spot after preparation of BN by a two-step boration-nitration process. Apart from the BN related (10) spot, no additional spots due the formation of a hexagonal BN/Rh superstructure can be observed, i.e., only the formation of small BN domains is expected.

190.6 eV and the N-1s intensity, the ratio is in the range of B:N$\sim$0.9:1, i.e., even without an intermediate oxidation, it is possible to transform part of the boron from the B-Rh compound into BN just by exposing it to NH_3. However, without intermediate oxidation, it is apparently not possible to extract the whole subsurface boron by simple exposure of the Rh surface NH_3. For the two-step process, the C-1s intensities are much higher than for the three-step process, since initial carbon impurities cannot be eliminated by the intermediate oxidation.

With respect to the surface structure, the portion of boron nitride that is formed during nitration exhibits just a low degree of order, compared to the hexagonal BN layer that is formed by the three-step process. The LEED profile in Fig. 16(b) displays an additional peak for the (10) spot at higher transfer of momentum, but this peak just appears as a diffuse structure. In contrast to the LEED profiles of the hexagonal BN film from the three-step process in Fig. 13(b) and 13(c), no additional spots due to the formation of a superstructure can be observed in Fig. 16. We therefore suppose that the average domain size of the BN film for the two-step process is only in the range of the periodicity of the BN/Rh coincidence lattice ($\sim$3.2 nm).

In general, it is possible to prepare hexagonal BN layers even by a two-step boration-nitration process, but this kind of preparation suffers from two deficiencies: First, it is not possible to transform all boron from the B-Rh species into BN-like species, second, the structural quality of the BN film cannot compete with that of the three-step process. Probably, it may be possible to improve the quality of the hexagonal BN layers even for the two-step process by optimizing the parameters of preparation, such as temperature, pressure or deposition time. However, since the three-step process provides hexagonal BN layers of nearly perfect structural quality, the application of the intermediate oxidation step seems to be preferable to the exploration of a multidimensional space of parameters.

IV. SUMMARY

In this study, we presented a novel route for the controlled preparation of a well-ordered hexagonal BN monolayer on a Rh(111) surface. The explored three-step boration-oxidation-nitration process clearly demonstrates that the formation of BN monolayers is also possible when boron and nitrogen are provided successively by different sources. This kind of preparation is in contrast to the current standard procedures for which the full structural motif of the BN monolayer, the $(BN)_3$ hexagon, is provided via the precursor (borazine or trichlorborazine). This new growth mechanism may offer the possibility for the preparation of multilayer BN or for the deposition of BN layers on metal surfaces that exhibit poor sticking coefficients for borazine precursors.

In addition, each individual step of the boration-oxidation-nitration process is also of particular scientific interest: (i) The full decomposition of the $B(OMe)_3$ precursor offers an easy access for embedding boron atoms on interstitials within the lattice of a metal substrate, a procedure that offers the possibility to prepare boride surfaces for wear resistant materials. (ii) The oxidation of the B-metal surface (here: B-Rh) results in an boron oxygen layer of a thickness of about 1 nm that may act as a small insulating barrier in a nanoelectronic device. (iii) The transformation of the boron oxygen layer into a hexagonal BN monolayer by nitration (the initial aim of this study) offers the possibility for large-scale, wafer-size production of well-ordered BN layers.

STM investigations similar to those presented in Ref. 40 may provide useful information with respect to the growth kinetics of our three-step mechanism and the structural quality of the resulting BN monolayers. In the study by Dong *et al.*[40] the growth of the BN nanomesh, as prepared by the standard CVD procedure using borazine, was probed *in situ* by time and temperature-dependent STM. It was shown that the defectiveness of the BN layers strongly depends on the interplay of surface diffusion and the number of nucleation centers, as given by the flux of the precursor. The authors proposed that the best quality of the BN nanomesh, if prepared by CVD of borazine, can be achieved by combining "a low flux and a high diffusion coefficient."[40] Similar studies for the present synthesis route would be highly desirable in order to find out the optimum concept for high quality BN nanomesh films.

ACKNOWLEDGMENTS

This work was supported by the European Specific Targeted Research Project "*Nanomesh*" (Grant No. NMP4-CT-2004-013817) and by the Deutsche Forschungsgemeinschaft within the Priority Program under Grant No. SPP 1164 *"Nano and Micro Fluidics."*

*Corresponding author.
†f.mueller@mx.uni-saarland.de
‡h.sachdev@mx.uni-saarland.de

[1] R. Laskowski, P. Blaha, T. Gallauner, and K. Schwarz, Phys. Rev. Lett. **98**, 106802 (2007).
[2] R. Laskowski and P. Blaha, J. Phys.: Condens. Matter **20**, 064207 (2008).
[3] M. Corso, W. Auwärter, M. Muntwiler, A. Tamai, T. Greber, and J. Osterwalder, Science **303**, 217 (2004).
[4] S. Berner, M. Corso, R. Widmer, O. Groening, R. Laskowski, P. Blaha, K. Schwarz, A. Goriachko, H. Over, S. Gsell, M. Schreck, H. Sachdev, T. Greber, and J. Osterwalder, Angew. Chem. **119**, 5207 (2007).
[5] H. Dil, J. Lobo-Checa, R. Laskowski, P. Blaha, S. Berner, J. Osterwalder, and T. Greber, Science **319**, 1824 (2008).
[6] A. J. Pollard, E. W. Perkins, N. A. Smith, A. Saywell, G. Goretzki, A. G. Phillips, S. P. Argent, H. Sachdev, F. Müller, S. Hüfner, S. Gsell, M. Fischer, M. Schreck, J. Osterwalder, T. Greber, S. Berner, N. R. Champness, and P. H. Beton, Angew. Chem. **122**, 1838 (2010).
[7] A. K. Geim and K. S. Novoselov, Nature Mater. **6**, 183 (2007).
[8] A. Nagashima, N. Tejima, Y. Gamou, T. Kawai, and C. Oshima, Surf. Sci. **357-358**, 307 (1996).
[9] H. Sachdev, F. Müller, and S. Hüfner, Diamond Relat. Mater. **19**, 1027 (2010). In analogy to the term *"graphene,"* as describing one monolayer of graphite with a honeycomb lattice, it is proposed to use the term *"boronitrene"* for the graphenelike hexagonal honeycomb lattice of boron nitride.
[10] F. Müller, S. Hüfner, and H. Sachdev, Surf. Sci. **603**, 425 (2009).
[11] F. Müller, S. Hüfner, and H. Sachdev, Surf. Sci. **602**, 3467 (2008).
[12] F. Müller, K. Stöwe, and H. Sachdev, Chem. Mater. **17**, 3464 (2005).
[13] A. B. Preobrajenski, A. S. Vinogradov, May Ling Ng, E. Cavar, R. Westerström, A. Mikkelsen, E. Lundgren, and N. Mårtensson, Phys. Rev. B **75**, 245412 (2007).
[14] M. Morscher, M. Corso, T. Greber, and J. Osterwalder, Surf. Sci. **600**, 3280 (2006).
[15] W. Auwärter, T. J. Kreutz, T. Greber, and J. Osterwalder, Surf. Sci. **429**, 229 (1999).
[16] W. Auwärter, H. U. Suter, H. Sachdev, and T. Greber, Chem. Mater. **16**, 343 (2004).
[17] W. Auwärter, M. Muntwiler, J. Osterwalder, and T. Greber, Surf. Sci. **545**, L735 (2003).
[18] J. Osterwalder, W. Auwärter, M. Muntwiler, and T. Greber, e-J. Surf. Sci. Nanotechnol. **1**, 124 (2003).
[19] M. Muntwiler, M. Hengsberger, A. Dolocan, H. Neff, T. Greber, and J. Osterwalder, Phys. Rev. B **75**, 075407 (2007).
[20] T. Greber, L. Brandenberger, M. Corso, A. Tamai, and J. Osterwalder, e-J. Surf. Sci. Nanotech. **4**, 410 (2006).
[21] M. T. Paffett, R. J. Simonson, P. Papin, and R. T. Paine, Surf. Sci. **232**, 286 (1990).
[22] M. Corso, T. Greber, and J. Osterwalder, Surf. Sci. **577**, L78 (2005).
[23] A. Goriachko, Y. He, M. Knapp, H. Over, M. Corso, T. Brugger, S. Berner, J. Osterwalder, and T. Greber, Langmuir **23**, 2928 (2007).

[24] M. P. Allan, S. Berner, M. Corso, T. Greber, and J. Osterwalder, Nanoscale Res. Lett. **2**, 94 (2007).
[25] O. R. Lourie, C. R. Jones, B. M. Bartlett, P. C. Gibbons, R. S. Ruoff, and W. E. Buhro, Chem. Mater. **12**, 1808 (2000).
[26] K. T. Moon, D. S. Min, and D. P. Kim, J. Ind. Eng. Chem. **3**, 288 (1997).
[27] F. Müller, R. de Masi, D. Reinicke, P. Steiner, S. Hüfner, and K. Stöwe, Surf. Sci. **520**, 158 (2002).
[28] R. de Masi, D. Reinicke, F. Müller, P. Steiner, and S. Hüfner, Surf. Sci. **515**, 523 (2002).
[29] R. de Masi, D. Reinicke, F. Müller, P. Steiner, and S. Hüfner, Surf. Sci. **516**, L515 (2002).
[30] F. Müller, H. Sachdev, S. Hüfner, A. J. Pollard, E. W. Perkins, J. C. Russell, P. H. Beton, S. Gsell, M. Fischer, M. Schreck, and B. Stritzker, Small **5**, 2291 (2009).
[31] S. Gsell, M. Fischer, M. Schreck, and B. Stritzker, J. Cryst. Growth **311**, 3731 (2009).
[32] J. Kiss, K. Révész, and F. Solymosi, Appl. Surf. Sci. **37**, 95 (1989).
[33] D. N. Hendrickson, J. M. Hollander, and W. L. Jolly, Inorg. Chem. **9**, 612 (1970).
[34] J. A. Schreifels, P. C. Maybury, and W. E. Swartz, J. Catal. **65**, 195 (1980).
[35] The details on the chemistry of the precursor decay will be discussed in a separate study, H. Sachdev, F. Müller, and S. Hüfner, Angew. Chem. (to be published).
[36] M. Elango, V. Subramanian, and N. Sathyamurthy, J. Phys. Chem. A **112**, 8107 (2008).
[37] H. Kohlmann, F. Müller, K. Stöwe, A. Zalga, and H. P. Beck, Z. Anorg. Allg. Chem. **635**, 1407 (2009).
[38] M. P. Seah and W. A. Dench, Surf. Interface Anal. **1**, 2 (1979).
[39] M. Romand and M. Roubin, Analysis **4**, 308 (1976).
[40] G. Dong, E. B. Fourré, F. C. Tabak, and J. W. M. Frenken, Phys. Rev. Lett. **104**, 096102 (2010).